Lattice Disorder, Electric Properties, and Magnetic Behavior of La 1 − x Na x MnO 3+ δ Manganites

ARTICLE *in* THE JOURNAL OF PHYSICAL CHEMISTRY B · MARCH 2003

Impact Factor: 3.3 · DOI: 10.1021/jp027015z

5 AUTHORS, INCLUDING:

Lorenzo Malavasi
University of Pavia
154 PUBLICATIONS **1,636** CITATIONS
SEE PROFILE

M. C. Mozzati
University of Pavia
134 PUBLICATIONS **1,322** CITATIONS
SEE PROFILE

Paolo Ghigna
University of Pavia
171 PUBLICATIONS **1,319** CITATIONS
SEE PROFILE

G. Flor
University of Pavia
155 PUBLICATIONS **1,236** CITATIONS
SEE PROFILE

Lattice Disorder, Electric Properties, and Magnetic Behavior of $La_{1-x}Na_xMnO_{3+\delta}$ Manganites

Lorenzo Malavasi,*,† Maria Cristina Mozzati,‡ Paolo Ghigna,† Carlo B. Azzoni,‡ and Giorgio Flor†

Dipartimento di Chimica Fisica "M. Rolla", INSTM, IENI/CNR Unità di Pavia of Università di Pavia, V. le Taramelli 16, I-27100, Pavia, Italy, and INFM, Unità di Pavia and Dipartimento di Fisica "A. Volta", Università di Pavia, Via Bassi 6, I-27100, Pavia, Italy

Received: September 17, 2002

$La_{1-x}Na_xMnO_{3+\delta}$ samples with well-defined cation molecularity and oxygen contents ($x = 0.05$, $x = 0.13$, and $-0.04 \leq \delta \leq 0.078$) are analyzed with XRPD, electrical conductivity, static magnetization, and EPR measurements. The majority defects induced by oxygen over- and under-stoichiometry are cation and oxygen vacancies; the cation vacancies affect the magnetic properties by interrupting the interaction paths between Mn(III) and Mn(IV) ions, whereas the oxygen vacancies have a stronger influence on the structural and electrical properties and act on the magnetic properties by the overall decrease of the Mn(IV) amount and by the creation of sample regions with different magnetic features. We can state that the basic magnetic and electrical behaviors of the Na-doped lanthanum manganite compounds are driven from the Mn(IV)/Mn(III) ratio and all the peculiar behaviors are indeed caused by defects, concentration gradient and, more generally, by lattice disorder.

1. Introduction

Rare earth manganite perovskites of general formula $Ln_{1-x}A_xMnO_3$ (Ln = La, Pr; A = Ca, Sr) are, at present, among the most studied materials due to their relevant properties such as the colossal magneto-resistance (CMR) effect and charge and spin order. The research efforts during these years have pointed out the role played by the different oxidation states, (III) and (IV), of the manganese ions; in $LaMnO_{3+\delta}$ and $La_{1-x}Ca_xMnO_3$ systems, for example, a Mn(IV) content around ∼30% was found to be the optimal value in order to achieve the maximum CMR effect and also the highest Curie temperature (T_c) for the paramagnetic-to-ferromagnetic transition (P−F).[1,2] In the magnetic ordered state the electron hopping process is favored by the spin arrangement while for temperatures above T_c the conduction mechanism is semiconducting-like. This behavior was closely related to the double-exchange (DE) mechanism, first proposed by Zener,[3] which involves the transfer of e_g electrons between neighboring Mn ions when these are ferromagnetically coupled. The DE mechanism alone does not allow a satisfactory description of the resistivity trend in these systems[4,5] and a more complete picture takes into account the electron−phonon coupling associated with the Jahn−Teller (J−T) effect.

Usually, the Mn(IV) amount is tuned by aliovalent cation doping on the A site. Another way to change the Mn(IV)/Mn(III) ratio is the variation of the oxygen content (δ) by controlling temperature (T) and oxygen partial pressure ($P(O_2)$) during annealing steps. Anyway, the effect of the δ-variation has a different nature with respect to the cation doping since it acts not only as a holes or electrons source but also by creating crystallographic defects.[6]

The defect chemistry of CMR manganites has been first considered for the undoped $LaMnO_{3+\delta}$ by Van Roosmalen et al.[7,8] They determined that pure lanthanum manganese oxide always presents an oxygen over-stoichiometry compensated by cation vacancies, equally distributed between lanthanum and manganese sites according to the following equilibrium:

$$\frac{1}{2}O_2 \rightleftarrows O_O^x + \frac{1}{3}V_{La}''' + \frac{1}{3}V_{Mn}''' + 2h^\bullet \qquad (1)$$

Neutron diffraction experiments confirmed this model, even though there is still some debate about the relative amount of the lanthanum and manganese vacancies.[7−9] It is to remark that the closed-packed arrangement of the perovskite structure does not allow the formation of interstitial oxygen.

Until now, very few papers[6−10] have been published which deal with the effect of oxygen content variation (δ) on the transport and magnetic properties of doped manganites above all as regards the study of alkali-doped compounds. Besides, few works tried to go deeper in the analysis of the role of the oxygen vacancies related to oxygen under-stoichiometry.

In this paper we report about the synthesis of a series of $La_{1-x}Na_xMnO_{3+\delta}$ samples with $x = 0.05$, $x = 0.13$, and $-0.04 \leq \delta \leq 0.078$, carefully characterized for what concerns the cation stoichiometry and the oxygen content. To study the effect of oxygen nonstoichiometry on the electric and magnetic properties, we combined X-ray powder diffraction investigation (XRPD) and electrical conductivity, static magnetization and electron paramagnetic resonance (EPR) measurements with the aim to point out that a complete understanding of the physical properties of doped perovskite manganites requires a rigorous control of the oxygen content, as already recognized in other functional oxides such as the high-temperature superconductors.

* Corresponding author. E-mail: malavasi@chifis.unipv.it.
† Dipartimento di Chimica Fisica "M. Rolla", INSTM, IENI/CNR Unità di Pavia of Università di Pavia.
‡ INFM, Unità di Pavia and Dipartimento di Fisica "A. Volta", Università di Pavia.

10.1021/jp027015z CCC: $25.00
Published on Web 02/20/2003

2. Experimental Section

$La_{1-x}Na_xMnO_{3+\delta}$ samples with $x = 0.05$ and $x = 0.13$ were synthesized by solid-state reaction starting from proper amounts of La_2O_3 (Aldrich, 99.999%), Mn_2O_3 (Aldrich, 99.999%), and Na_2CO_3 (Aldrich, 99.99%). Pellets were prepared from the thoroughly mixed powders and allowed to react at 1173 K for a total time of at least 90 h, during which they were re-ground and re-pelletized at least twice. Low reaction temperature and long firing times have been chosen in order to avoid Na evaporation during the synthesis procedure.

X-ray powder diffraction patterns were acquired on a Philips 1710 diffractometer equipped with a Cu anticathode, adjustable divergence slit, graphite monochromator on the diffracted beam, and proportional detector. The lattice constants were determined by minimizing the weighted squared difference between calculated and experimental Q_i values, where $Q_i = 4 \sin^2\theta_i/\lambda_i^2$ and weight $= \sin(2\theta_i)^{-2}$. Instrumental aberrations were considered by inserting additional terms into the linear least-squares-fitting model.[11]

Electron microprobe analysis (EMPA) measurements were carried out using an ARL SEMQ scanning electron microscope, performing at least 10 measurements in different regions of each sample. EMPA measurements were realized both on the as-prepared samples and on all the samples after the thermal treatments required, following the thermogravimetry results, to obtain the desired oxygen content. According to EMPA and XRPD data, the above synthetic procedure gave single-phase materials; in addition, each sample was found to be highly homogeneous in the chemical composition, which was met in fair agreement with the nominal one.

Thermogravimetric measurements were used to determine the oxygen content according to a method previously described.[12] These measurements have been performed under different atmospheres (obtained by flowing into the apparatus certified mixtures of oxygen in nitrogen) at 1123 K with a TA 2950 thermal analysis system. The as-prepared polycrystalline samples have been annealed at 1123 K and at $P(O_2) = 1$, 10^{-3}, and 10^{-5} atm to achieve, according to the thermogravimetric data, the following δ-values: $\delta = 0.078$, 0, and -0.01 for $x = 0.05$; $\delta = 0$, -0.03, and -0.04 for $x = 0.13$.

DC conductivity measurements were performed by means of an Amel 55 galvanostat and a Keithley 180 nanovoltmeter, using the four-probe DC method, on samples shaped in the form of parallelepipeds, in a Leybold ROK cryostat.

Static magnetic susceptibility was measured at 100 Oe from 350 K down to 2 K with a SQUID magnetometer (Quantum Design).

EPR measurements in X band (~9.5 GHz) were performed with a Bruker spectrometer, with a continuous nitrogen flow apparatus and suitable resonant cavities, to study the temperature dependence in the range 120−700 K.

3. Results

The oxygen content at 1123 K for the samples considered in this work, $La_{0.95}Na_{0.05}MnO_{3+\delta}$ and $La_{0.87}Na_{0.13}MnO_{3+\delta}$, is shown in Figure 1 as a function of the logarithm of the oxygen partial pressure, $P(O_2)$. By increasing the Na doping, the oxygen content reduces for the same T and $P(O_2)$ values. In detail, for the $x = 0.05$ samples it is possible to note that in pure oxygen the material is over-stoichiometric ($\delta = 0.078$), while by reducing the $P(O_2)$ an oxygen under-stoichiometry is achieved at 10^{-5} atm ($\delta = -0.01$). On the other hand, for $x = 0.13$ the material is stoichiometric in the oxygen content at $P(O_2) = 1$ atm and under-stoichiometric for the lower $P(O_2)$.

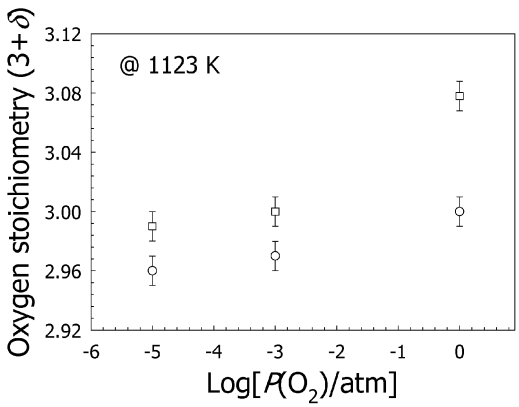

Figure 1. Oxygen content vs the logarithm of the oxygen partial pressure ($P(O_2)$) for $La_{1-x}Na_xMnO_{3+\delta}$ with $x = 0.05$ (open squares) and $x = 0.13$ (open circles).

In the present case, the Na doping can be rationalized by considering the following quasi-chemical equilibrium:

$$Na_2O + 2La_{La} + 6O_O \rightleftarrows 2Na''_{La} + La_2O_3 + 2V^{\bullet\bullet}_O + 4O_O \quad (2)$$

and the oxygen vacancies annihilation with the external atmosphere:

$$2V^{\bullet\bullet}_O + O_2 \rightleftarrows 2O_O + 4h^{\bullet} \quad (3)$$

These holes are responsible for the formation of Mn(IV) ions:

$$Mn(III) + h^{\bullet} \rightleftarrows Mn(IV) \quad (4)$$

It is therefore clear that the formation of oxygen vacancies leads to the annihilation of Mn(IV). In addition, for a given Na doping level x, the density of Mn(IV), expressed as number per unit formula, is given by

$$[Mn(IV)] = 2(x + \delta) \quad (5)$$

where δ is intended as negative in the presence of oxygen vacancies. The oxygen content should very deeply affect the structural, transport, and magnetic properties of the Na-doped lanthanum manganites both by directly supplying charge carriers (holes or electrons) and by creating lattice defects (cation or anion vacancies).

Figure 2 reports the X-ray powder diffraction (XRPD) patterns for the samples with $x = 0.05$ and $\delta = 0.078$, 0, and -0.01 and for the samples with $x = 0.13$ and $\delta = 0$, -0.03, and -0.04. For $x = 0.05$ the crystal structure is orthorhombic when $\delta = 0$ and $\delta = -0.01$ and can be indexed according to the *Pnma* structure (space group n. 62) while for $\delta = 0.078$ the crystal structure is more symmetric, belonging to the rhombohedric $R\bar{3}c$ space group. Moreover, for $La_{0.95}Na_{0.05}MnO_{2.99}$ the lattice parameters ratio ($c/a < \sqrt{2}$) suggests the presence of a static cooperative Jahn−Teller deformation of the octahedra array in which the $(x^2-y^2)e_g$ orbital ordering takes place and induces an extension of the unit cell in the $a-b$ plane.[13] In this case, the crystal structure is designated as orthorhombic O′. For the sample $La_{0.95}Na_{0.05}MnO_3$, $c/a \sim \sqrt{2}$, thus suggesting the evolution toward a dynamic J−T deformation by increasing the oxygen content. This structure is defined as orthorhombic O. For $x = 0.13$ all the samples are rhombohedric. The corresponding lattice constants and cell volumes are reported in Table 1 for all the samples.

By looking at the cell volumes of Table 1 it is possible to note that by increasing the sodium content, for the same oxygen

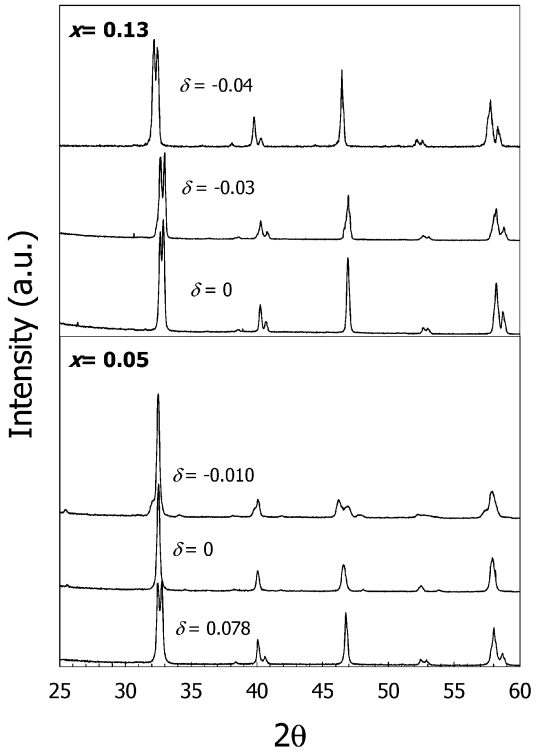

Figure 2. X-ray powder patterns for $La_{1-x}Na_xMnO_{3+\delta}$ with $x = 0.05$ (bottom) and $x = 0.13$ (top).

content, the cell dimension reduces and by increasing the oxygen content, at fixed *x*, the cell volume reduces too. Since the ionic radii of La(III) (1.39 Å) and Na(I) (1.36 Å), for the same coordination, are very close,[14] this reflects the progressive increase of the Mn(IV)/Mn(III) ratio by increasing δ and/or *x* being the ionic radii 0.645 Å and 0.53 Å for Mn(III) and Mn(IV), respectively.[14] This allowed us to concentrate mainly on the role of the oxygen nonstoichiometry effect and less to the effect of the average ionic radius of the A site responsible of the Mn−O bandwidth[15] through the tolerance factor *t*. *t* represents a measure of the mismatch of the equilibrium (Mn−O) and (A−O) bond lengths:[16] usually, the $AMnO_3$ structure adjusts to $t < 1$ by cooperative rotations of the MnO_6 octahedra along different crystal axes; these rotations create Mn−O−Mn bond angles < 180°. The evolution from an orbitally ordered orthorhombic structure to a rhombohedric one, as the cation doping or/and oxygen over-stoichiometry increases, reflects the progressive decrease of J−T Mn(III) ions, the subsequent reduction of (Mn−O) bond length and the approach to 180° of Mn−O−Mn bond angle which is the optimal condition for the charge carrier hopping.[1]

Figure 3 presents the plot of the electrical resistivity (ρ) as a function of temperature for the $La_{0.95}Na_{0.05}MnO_{3+\delta}$ samples. Measurements were performed in a reduced temperature range because of the high resistivity values. As can be inferred, all the samples present an activated transport. Only for the highest

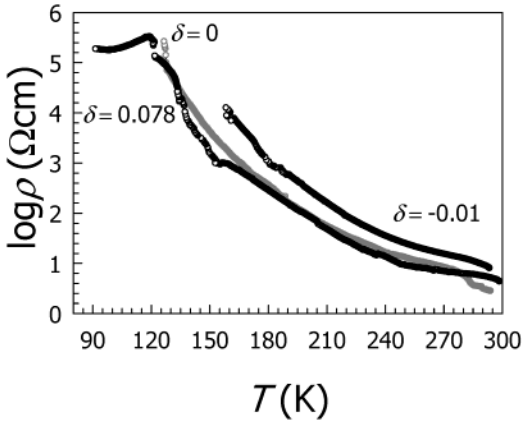

Figure 3. Logarithm of electrical resistivity vs temperature for $x = 0.05$ samples.

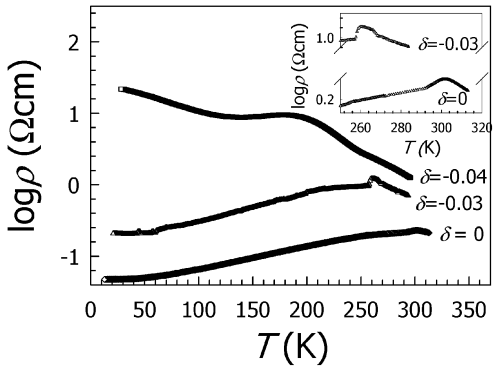

Figure 4. Logarithm of electrical resistivity vs temperature for $x = 0.13$ samples. The inset evidences the transition zone for $\delta = 0$ and $\delta = -0.03$.

oxygen content ($\delta = 0.078$) a transition to a metallic-like conductivity is detectable at $T_\rho \sim 120$ K. Despite the large difference in the Mn(IV) content, the samples with $\delta = 0.078$ and $\delta = 0$ display similar ρ-values, lower than that of the under-stoichiometric sample.

Figure 4 reports the ρ vs *T* behavior for the samples with $x = 0.13$. The samples with $\delta = 0$ and $\delta = -0.03$ show a clear transition from a semiconducting-like (activated) regime to a metallic-like one (S−M) at $T_\rho \sim 303$ K and $T_\rho \sim 260$ K, respectively (as determined from the derivative of the $\rho(T)$ curve). The third sample ($\delta = -0.04$) displays a transition as well, even if broader than in the former case, between two activated regimes. Let's note that this sample is the one with the highest oxygen under-stoichiometry.

The semiconducting-like regime, dominated by the charge carriers trapping phenomena related to lattice distortions and/or defects, has been analyzed be means of an adiabatic small-polaron model, according to[17]

$$\rho = \rho_0 T \exp(E_a/k_B T) \qquad (6)$$

in which the electron-transfer time is lower with respect to the transfer time of the atomic polarization between adjacent sites.

TABLE 1: Lattice Parameters (*a*, *b*, and *c*), Cell Volumes (*V*), Transition Temperatures (T_ρ and T_c), Activation Energies (E_a), and Estimated Mn(IV) Contents for the Samples Considered in the Paper

sample	*a* (Å)	*b* (Å)	*c* (Å)	*V* (Å^3)	T_ρ (K)	T_c (K)	E_a (meV)	% Mn(IV)
$La_{0.95}Na_{0.05}MnO_{3.078}$	5.514	5.514	13.328	58.49	120	117 ± 5	210	26
$La_{0.95}Na_{0.05}MnO_3$	5.517	5.534	7.785	59.43		152 ± 5	196	10
$La_{0.95}Na_{0.05}MnO_{2.99}$	5.525	5.587	7.753	59.83		112 ± 5	235	8
$La_{0.87}Na_{0.13}MnO_3$	5.512	5.512	13.351	58.54	303	305	72	26
$La_{0.87}Na_{0.13}MnO_{2.97}$	5.533	5.533	13.366	59.06	260	267	105	20
$La_{0.87}Na_{0.13}MnO_{2.96}$	5.535	5.535	13.370	59.12	195	265	138	18

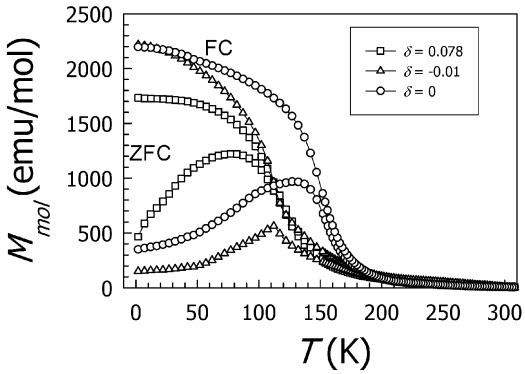

Figure 5. ZFC and FC molar magnetization at 100 Oe for the $x = 0.05$ samples.

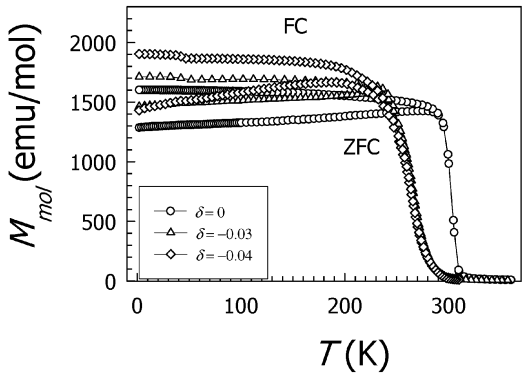

Figure 6. ZFC and FC molar magnetization at 100 Oe for the $x = 0.13$ samples.

The activation energies (E_a), as deduced by eq 6 for the charge carrier hopping are reported in Table 1.

For the $La_{0.95}Na_{0.05}MnO_{3+\delta}$ samples, the E_a values range around 200 meV. It is interesting to note, anyhow, that the sample with the lowest Mn(IV) content and oxygen vacancies shows the highest E_a value. For the $La_{0.87}Na_{0.13}MnO_{3+\delta}$ samples the activation energies are smaller, as a consequence of the less distorted crystal structure which enables an easier polaron dynamic. Moreover, a clear trend with the oxygen content may be now emphasized.

The metallic-like regime has been fitted according to the current model applied to the study of charge transport in perovskite manganites[2,18] by following the empirical expression

$$\rho = \rho_0 + \rho_2 T^2 + \rho_{4.5} T^{4.5} \qquad (7)$$

where ρ_0 represents the T-independent contribution to ρ, due mainly to grain boundaries and point-defects; the term $\rho_2 T^2$ takes into account the electron−electron scattering processes while the $\rho_{4.5} T^{4.5}$ term considers the electron−magnon interaction. The fit, performed for $T/T_\rho < 0.85$, to be sure of the completion of the transition, for the samples with $x = 0.13$ and $\delta = 0$ and $\delta = -0.03$ shows a general increase of all the parameters by reducing the oxygen content: $\rho_0 = 0.044$ and 0.184 Ω cm; $\rho_2 = 2.25$ and 11.6×10^{-6} Ω cm K^{-2}; and $\rho_{4.5} = 2.3$ and 5×10^{-12} Ω cm $K^{-4.5}$, respectively.

Figures 5 and 6 present the static magnetization (M) behavior vs T for the $La_{0.95}Na_{0.05}MnO_{3+\delta}$ and $La_{0.87}Na_{0.13}MnO_{3+\delta}$ series, respectively. Field cooling (FC) and zero-field cooling (ZFC) measurements were performed at 100 Oe. For all the samples a transition from a paramagnetic to a ferromagnetic phase (P−F) occurs. The Curie temperatures (T_c), taken at the inflection points in the FC curves, are reported in Table 1.

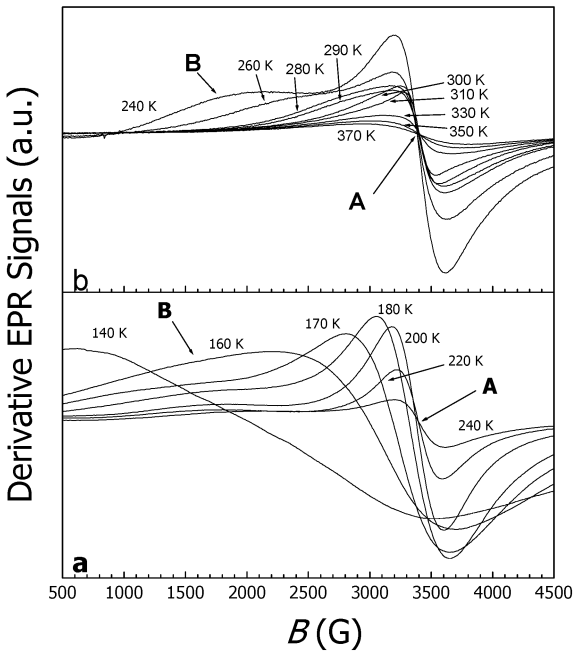

Figure 7. Temperature behavior of the derivative EPR signals of the A and B regions of the $x = 0.05$ and $\delta = 0$ sample. In (b) the signal intensity is amplified by a factor 5.

In detail, for the $x = 0.05$ samples the maximum T_c value is achieved for the sample with $\delta = 0$ (152 K) while for the other two samples the T_c are very close each other. Thus, an easy trend of T_c vs δ, and consequently vs the Mn(IV) content, does not hold; the induced defects strongly influence the T_c values, nearly irrespectively of the Mn(IV) amount. The shape of the ZFC curves (Figure 5) suggests the presence of magnetic domains, randomly oriented when cooling without an applied magnetic field. This is particularly evident for the understoichiometric sample ($\delta = -0.01$). Finally, let us note the relative broadness of the magnetic transitions for these samples.

The $La_{0.87}Na_{0.13}MnO_{3+\delta}$ samples show sharper magnetic transitions and reduced differences between FC and ZFC curves (Figure 6) compared to the $x = 0.05$ ones. The highest T_c pertains to the sample with the correct oxygen stoichiometry, i.e., defects free, which is also the one with the sharpest P−F transition and the smallest difference between FC and ZFC curves. The other two samples have approximately the same T_c even if the sample with the greater oxygen vacancies content, $\delta = -0.04$, displays a greater difference between FC and ZFC curves.

The EPR measurements can aid in deepening the comprehension of the magnetic behavior, particularly when approaching the magnetic transition. In lanthanum manganites the EPR signal may arise from Mn(IV) single ions or from Mn(III)−Mn(IV) Zener pairs:[19] in both cases, in the paramagnetic phase, a signal centered at $g \cong 2$ is expected.

A common behavior has been found for the EPR signals of all $La_{1-x}Na_xMnO_{3+\delta}$ samples. A selected example is shown in Figure 7 where the EPR signal vs T of the sample with $x = 0.05$ and $\delta = 0$ is reported. Shortly, for temperatures lower than a T_L value only one signal is observed with $g_{eff} > 2$, thus evidencing the presence of internal magnetic fields resulting from ferromagnetic ordering in the whole sample; for temperatures higher than a T_H value only one signal with $g \cong 2$ is present, suggesting the paramagnetic character of the whole sample; in the intermediate temperature range, $T_H - T_L \equiv \Delta T_c$, at least two distinct signals, with different trends vs T, are detectable.

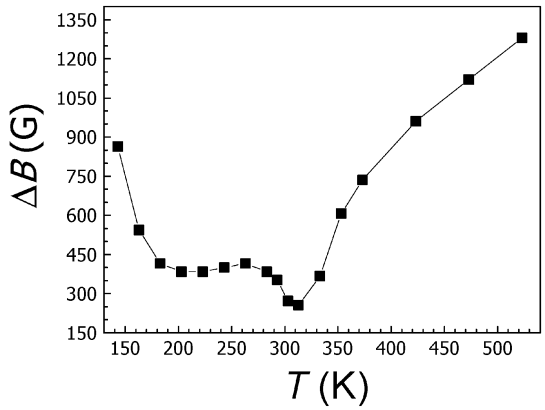

Figure 8. EPR line width behavior vs T for the $x = 0.05$ and $\delta = 0.78$ sample.

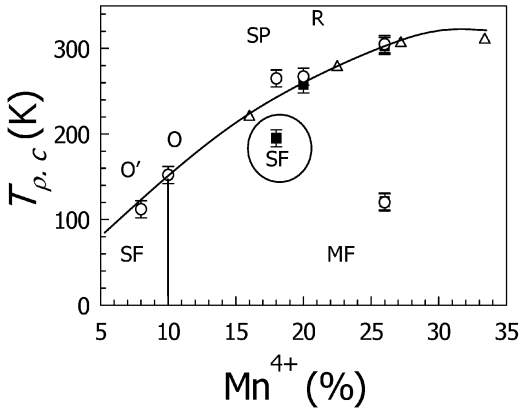

Figure 9. Transition temperatures (T_ρ and T_c) vs Mn^{4+} content; O and R refer to the orthorhombic and rhombohedric crystal structure, respectively; SP means semiconducting-paramagnet; SF, semiconducting-ferromagnet; and MF metallic-ferromagnet. T_ρ (full squares), T_c (empty circles), and T_c taken from ref [24] (empty triangles).

In detail, for the samples with $x = 0.05$, two magnetic regions (here named A and B) in which the long-range magnetic interactions hold until different temperatures, T_A and T_B, are evident. For $\delta = 0.078$ ($T_L < 140$ K) $T_A \cong 200$ K and $T_B \cong 330$ K; for $\delta = 0$ ($T_L \cong 140$ K) $T_A \cong 240$ K and $T_B \cong 330$ K; for $\delta = -0.01$ ($T_L \cong 140$ K) $T_A \cong 330$ K and $T_B \cong 600$ K.

Concerning the samples with $x = 0.13$, for $\delta = 0$ two EPR signals are observed at the lowest investigated temperature (293 K) corresponding to two different magnetic regions, with $T_A <$ 293 K and $T_B = 310$ K, which rapidly merge: at 310 K the sample shows a pure paramagnetic behavior. Analogous features can be observed for the other samples with $x = 0.13$ and with $\delta = -0.03$ ($T_L = 260$ K, $T_A = 270$ K, $T_B = 300$ K) and $\delta = -0.04$ ($T_L = 250$ K, $T_A = 255$ K, $T_B = 300$ K).

By assuming $T_H = T_B$, we point out that the ΔT_c range corresponds well to the onset and completion of the magnetic transition and its extent agrees with the broadening of the magnetic transition. For the same x-values, the extent of ΔT_c strongly depends on the oxygen vacancies. Indeed, the narrowest ΔT_c value corresponds to the samples with the correct oxygen content, i.e., $\delta = 0$, whereas wider transitions are observed for the samples with $\delta < 0$. For $x = 0.13$, the temperature range of the coexistence of the two EPR signals is highly reduced with respect to the samples with $x = 0.05$. The multiplicity of EPR signals suggests the presence, in the samples, of different magnetic regions: for $\delta = 0$ they are mainly due to Mn(IV) concentration gradients, more evident for low Mn(IV) concentration; when $\delta \neq 0$ they also arise from possible inhomogeneous defects distribution.

For the $x = 0.13$ samples, the EPR signals show the main features already observed in analogous CMR calcium manganites with $x = 0.33$, that is with a nearly equal amount of Mn(IV).[20−23] Shortly, by lowering the temperature the EPR line width (ΔB) linearly decreases and reaches its minimum value at a temperature, named $T_{onset} \sim T_B$, greater than T_c. For $T < T_{onset}$, ΔB increases.[20,21,23] Opposite, for $x = 0.05$, the ΔB vs T trend is more complex as a consequence of the extent of the temperature range (ΔT_c) where the two different magnetic regions coexist. Indeed, two minima, corresponding well to T_A and T_B, are present as evidenced in Figure 8 for the $\delta = 0.078$ sample, selected as an example.

The EPR measurements allow also relating the magnetic behavior in the critical region (ΔT_c) to $\rho(T)$ peaks and slope variations. They can be associated to the T_A and T_B transition temperatures: indeed, we can observe a peak at ∼300 K for the sample with $x = 0.13$ and $\delta = 0$, a peak at ∼270 K for the sample with $x = 0.13$ and $\delta = -0.03$, and the slope change at 250 K for the sample with $x = 0.13$ and $\delta = -0.04$. So, the complex $\rho(T)$ behavior is also justified from the sample nonhomogeneity.

4. Discussion and Conclusions

The whole set of results we gained by this experimental study can be better focused by presenting the data as a phase diagram (Figure 9) in which T_ρ and T_c are plotted against the Mn(IV) content, as estimated by the oxygen and cation stoichiometry. Data from ref 24 are also reported.

The crystal structure evolves from an orbitally ordered, highly distorted, orthorhombic to a less distorted rhombohedric one by increasing the Mn(IV) content, i.e., by decreasing the J−T Mn(III) ions, irrespective that this is created by the oxygen overstoichiometry or by the Na-doping.

In the orthorhombic phase, a semiconducting transport mechanism is always observed. The activation energy values (Table 1) confirm the known close correlation between the polaronic hopping and the crystal structure, particularly with the Mn−O bond lengths and Mn−O−Mn bond angle; moreover, a close correlation can now also be established with the presence of lattice defects created by the oxygen nonstoichiometry.

For the $La_{0.95}Na_{0.05}MnO_{3+\delta}$ samples, the lowest E_a value corresponds to the stoichiometric sample (defect-free) while the introduction of anion vacancies ($\delta = -0.01$) increases the E_a. For the over-stoichiometric sample ($\delta = 0.078$) despite a rhombohedric structure and a relatively high Mn(IV) amount, the charge carrier hopping is little hindered by the presence of about 2.5% cation vacancies on the manganese site. Anyway, this is the only sample of this series which shows the insurgence of a S−M transition ($T_\rho = 120$ K) even if the high defect concentration makes the residual resistivity high. For all these samples, anyway, a magnetic P−F transition can be detected. The maximum T_c value (Table 1) corresponds to the sample with $\delta = 0$ (152 K) with a Mn(IV) content of about 10%. Let's note that for an analogous doping level, in an oxygen stoichiometric sample for the La−Ca−Mn−O system, T_c is about 155 K.[2] The introduction of anion vacancies according to equilibrium 2 causes a reduction of T_c to 112 K. For the over-stoichiometric sample, the relatively high amount of cation vacancies, introduced in accordance with equilibrium 1, causes, as well, a reduction of T_c to 117 K. The shape of the magnetization curves again indicates the crucial role of the defects introduced by the oxygen nonstoichiometry, the greater difference between FC and ZFC curves pertaining to the under-stoichiometric sample of the $x = 0.05$ series.

As regards the $La_{0.87}Na_{0.13}MnO_{3+\delta}$ samples, the increased intrinsic cation doping makes all of them rhombohedric. The more symmetric structure enables an easier polaron hopping which results in lower E_a values with respect to the $x = 0.05$ samples. Among the $x = 0.13$ samples, the one without point defects ($\delta = 0$) allows the easiest carrier motion; moreover, this is also the sample with the highest T_ρ (303 K) and the sharper S−M transition. The creation of anion vacancies reduces T_ρ to 260 K for the sample with $\delta = -0.03$, which displays as well a sharp S−M transition, while the further reduction of oxygen content ($\delta = -0.04$) inhibits the S−M transition and leads to a broad transition with $T_\rho = 195$ K between two semiconducting regimes. Also, for all these samples a P−F transition is observed in the magnetization curves. For $\delta = 0$ and $\delta = -0.03$, T_c is close to T_ρ while for $\delta = -0.04$ a discrepancy is observed. For the lowest oxygen content, anyway, the greater difference in the FC-ZFC curves is detected.

The main conclusion we can draw from the transport and magnetic data is that the anion vacancies seem to primarily influence the transport properties by both annihilating Mn(IV) ions and creating trapping centers and lattice distortion for the charge carriers. Besides, anomalous $\rho(T)$ behaviors can be ascribed to different responses of the sample regions and the overall decrease of conductivity can be also due to region boundary effects. This is consistent with the ΔT_c extent and the differences between ZFC and FC $M(T)$ curves, more relevant for the samples with $\delta < 0$, indicating the presence of separated samples regions, with different T_c values and with different $\rho(T)$ behaviors, as proved by the relation between the EPR T_A and T_B and peaks and slope changes in the $\rho(T)$ curves.

Completely different is the role of cation vacancies. We characterized two samples with the same "nominal" Mn(IV) content (26%): $x = 0.13$ and $\delta = 0$, $x = 0.05$ and $\delta = 0.078$. The first sample, practically defects free, as told above, shows the highest T_ρ and T_c and the lowest resistivity values. For the other sample, the great oxygen over-stoichiometry results in a large amount of cation vacancies. The vacancies on the Mn site can interrupt the magnetic interaction paths between Mn(III) and Mn(IV) ions, thus giving rise to the observed decrease of the T_c.

In conclusion, in this paper we have shown the role of oxygen nonstoichiometry induced defects, i.e., oxygen vacancies or cation vacancies, on the structural, transport, and magnetic properties of sodium-doped lanthanum manganites. The cation vacancies mainly affect, in direct way, the magnetic interactions whereas the oxygen vacancies have a stronger influence on the electrical properties and act on the magnetic properties by the overall decrease of the Mn(IV) amount and by the creation of sample regions with different magnetic features due to the lattice unhomogeneity. Finally, for highly distorted lattices and with a high concentration of defects, we cannot exclude the trapping of electron/holes in the anionic/cationic vacancies which may reduce the actual Mn(IV) content, with respect to that evaluated from δ and x-values. These defects cannot be detected by EPR in these samples due to their typical g-value ($g \cong 2$), corresponding to the Mn(IV) or Zener pairs one. Moreover, clustering phenomena of Mn(III)/Mn(IV) pairs may induce complex behavior of the charge carriers, as also observed in.[6,15,25]

In light of what we have seen, we can state that the basic magnetic and electrical behaviors of the Na-doped lanthanum manganite compounds are driven from the Mn(IV)−Mn(III) ratio and all the peculiar behaviors are indeed caused by defects, concentration gradient, and more generally by lattice disorder.

Acknowledgment. Dr. Simona Bigi is gratefully acknowledged for having performed EMPA analysis. The Department of earth science of Modena University and CNR of Modena are acknowledged for allowing SEM use. E. Jarosewich has kindly supplied the lanthanum standard for EMPA measurements. Dr. Giordano Paniconi is acknowledged for sample preparation. Dr. Oscar Barlascini is acknowledged for the assistance with EPR measurements.

References and Notes

(1) Mahendiran, R.; Tiwary, S. K.; Raychaudhuri, A. K.; Ramakrishnan, T. V.; Mahesh, R.; Rangavittal, N.; Rao, C. N. R. *Phys. Rev. B* **1996**, *53*, 3348.

(2) Schiffer, P.; Ramirez, A. P.; Bao, W.; Cheong, S. W. *Phys. Rev. Lett.* **1995**, *75*, 3336.

(3) Zener, C. *Phys. Rev.* **1951**, *82*, 403.

(4) Millis, A. J.; Littelwood, P. B.; Shraiman, B. I. *Phys. Rev. Lett.* **1995**, *74*, 5144.

(5) Röder, H.; Zang, J.; Bishop, A. R. *Phys. Rev. Lett.* **1996**, *76*, 1356.

(6) Vergara, J.; Ortega-Hertogs, R. J.; Madruga, V.; Sapiña, F.; El-Fadii, Z.; Martinez, E.; Beltrán, A.; Rao, K. V. *Phys. Rev. B* **1999**, *60*, 1127.

(7) van Roosmalen, J. A. M.; Cordfunke, E. H. P. *J. Solid State Chem.* **1991**, *93*, 212.

(8) van Roosmalen, J. A. M.; Cordfunke, E. H. P.; Helmholdt, R. B.; Zandbergen, H. W. *J. Solid State Chem.* **1994**, *110*, 100.

(9) De Souza, R. A.; Islam, M. S.; Ivers-Tiffée, E. *J. Mater. Chem.* **1999**, *9*, 1621.

(10) Herrero, E.; Alonso, J.; Martinez, J. L.; Vallet-Regt, M.; Gonzales-Calbet, J. M. *Chem. Mater.* **2000**, *12*, 1060.

(11) Spinolo, G.; Maglia, F. *Powder Diffraction* **1999**, *14*, 208.

(12) Ghigna, P.; Spinolo, G.; Malavasi, L.; Chiodelli, G.; Flor, G. *Phys. Chem. Chem. Phys.* **2001**, *3*, 606.

(13) Goodenough, J. B. Localized to itinerant electronic transition in perovskite oxides. *Structure and Bonding*; Springer-Verlag: Berlin, 2001; p 98.

(14) Shannon, R. D.; Previtt, C. T. *Acta Crystallogr.* **1970**, *B26*, 1046.

(15) Töpfer, J.; Goodenough, J. B. *Chem. Mater.* **1997**, *9*, 1467.

(16) Raveau, B.; Maignan, A.; Martin, C.; Hervieu, M. *Chem. Mater.* **1998**, *10*, 2641.

(17) Tuller, H. L.; Nowick, A. S. *J. Phys. Chem. Solids* **1977**, *38*, 859.

(18) Liu, X.; Zhu, H.; Zhang, Y. *Phys. Rev. B* **2002**, *65*, art. 024412.

(19) Oseroff, S. B.; Torikachvili, M.; Singley, J.; Ali, S.; Cheong, S.-W.; Schultz, S. *Phys. Rev. B* **1996**, *53*, 6521.

(20) Causa, M. T.; Tovar, M.; Caneiro, A.; Prado, F.; Ibañez, G.; Ramos, C. A.; Butera, A.; Alascio, B.; Obradors, X.; Piñol, S.; Rivadulla, F.; Vázquez-Vázquez, C.; López-Quintela, M. A.; Rivas, J.; Tokura, Y.; Oseroff, S. B. *Phys. Rev. B* **1998**, *58*, 3233.

(21) Rettori, C.; Rao, D.; Singley, J.; Kidwell, D.; Oseroff, S. B.; Causa, M. T.; Neumeier, J. J.; McClellan, K. J.; Cheong, S.-W.; Schultz, S. *Phys. Rev. B* **1997**, *55*, 3083.

(22) Yuan, S. L.; Li, G.; Jiang, Y.; Li, J. Q.; Zeng, X. Y.; Yang, Y. P.; Huang, Z.; Jin, S. Z. *J. Phys.: Condens. Matter* **2000**, *12*, L109.

(23) Yuan, S. L.; Li, J. Q.; Li, G.; Jiang, Y.; Zeng, X. Y.; Yang, Y. P.; Jin, S. Z. *J. Phys.: Condens. Matter* **2000**, *12*, L241.

(24) Roy, S.; Guo, Y. Q.; Venkatesch, S.; Ali, N. *J. Phys.: Condens. Matter* **2001**, *13*, 9547.

(25) Goodenough, J. B. *J. Appl. Phys.* **1997**, *81* (8), 5330.